Journal of Advanced Joining Processes 8 (2023) 100155

Contents lists available at ScienceDirect

Journal of Advanced Joining Processes

journal homepage: www.sciencedirect.com/journal/journal-of-advanced-joining-processes

Double-flush riveting by punching and compression

R.F.V. Sampaio [a], P. Larue [b], J.P.M. Pragana [a], I.M.F. Bragança [a,c], C.M.A. Silva [a], P.A.F. Martins [a,*]

[a] IDMEC, Instituto Superior Técnico, Universidade de Lisboa, Portugal
[b] ENSEIRB-MATMECA, Bordeaux INP, Talence, France
[c] CIMOSM, Instituto Superior de Engenharia de Lisboa, Instituto Politécnico de Lisboa, Portugal

ARTICLE INFO

Keywords:
Lap joints
Double-flush riveting
Process sequence
Simulation
Experimentation

ABSTRACT

This paper presents a new double-flush riveting process to fabricate flat lap joints that can be easily integrated in progressive or transfer multistage tool systems. The process is based on a punching-compression sequence and the design methodology combines experimentation and finite element modeling followed by destructive peel testing. Special emphasis is placed on the identification and selection of punch-to-die clearances to produce tapered cut surfaces that are appropriate for subsequent compression of the solid rivets into double-flush riveted lap joints. Results confirm that rivet materials with lower mechanical resistance than the sheet materials allow fabricating double-flush riveted lap joints with flat surfaces on both sides in which the mechanical interlocking in the undercut area is obtained by plastic deformation of the rivets instead of the sheets. The utilization of aluminum sheets and copper rivets allows extending the process scope of application from structural to energy distribution parts in which the electrical resistance of joints is a critical design parameter.

Introduction

Joining refers to a wide range of manufacturing technologies by which two or more individual parts can be permanently or temporarily assembled into a complete and useful single part, with or without the utilization of external elements, and with or without the application of heat or pressure. In the case of lap joints in which two sheets overlap, the commonly used technologies can be classified into four main groups, as shown in Fig. 1.

Welding is a manufacturing technology that ensures a continuous, permanent connection with a strength analogous to that of the individual overlapping sheets to be joined. The number of processes belonging to this group is large but their characteristics and the combinations of materials that can be successfully welded raise multiple problems, such as the difficulty of joining dissimilar materials and the metallurgical changes, residual stresses and distortions induced by the heat-cooling cycles. These problems are responsible for degradation in quality, loss in accuracy, and poor reliability of the lap joints, all leading to limits on the overall applicability of welding.

Brazing and soldering are manufacturing technologies that make use of hot filler materials, which upon solidification produce a continuous, permanent connection between the surfaces of the sheets to be joined. They can overcome some of above-mentioned problems of welding because it is only the filler material that is melted, but at the price of reducing the overall strength of the lap joints. Soldering, which is carried out at lower temperatures than brazing, gives rise to lap joints with the lowest strengths. Two other aspects that reduce the overall productivity of brazing and soldering is the preparation of the surfaces to be joined, which need to be chemically and mechanically cleaned, and the utilization of special fixtures to hold the sheets together with very tight tolerances so that the liquid filler materials are properly distributed between the mating sheet surfaces by capillary action.

Bonding is a manufacturing technology that makes use of thin films of liquid or semi-solid structural adhesives to produce a continuous, semi-permanent connection between the overlapping sheets. It overcomes the difficulties in connecting dissimilar materials, and in avoiding the metallurgical and dimensional changes of welding, brazing, and soldering, but raises new requirements and problems that have a negative impact on the productivity and scope of applicability. This is because the mating sheet surfaces must be carefully prepared and fixed in position under pressure until the adhesive is fully cured, and because the performance of adhesives over time is strongly influenced by the environmental working conditions (e.g., adhesives are negatively influenced by prolonged exposure to moist environments). A

* Corresponding author.
E-mail address: pmartins@tecnico.ulisboa.pt (P.A.F. Martins).

https://doi.org/10.1016/j.jajp.2023.100155

Available online 7 September 2023

comprehensive survey on the different types of lap joints fabricated by welding, brazing, soldering, and bonding can be found in Brandon and Kaplan (1997).

Mechanical joining (Fig. 1a) is a broader manufacturing technology group that includes joining by forming and fastening. Joining by forming includes a vast number of processes that make use of form-closed, force-closed, and material-closed mechanisms to connect two or more overlapped sheets in numerous ways, with or without the use of auxiliary joining elements (Meschut et al., 2022). Self-pierce riveting (Li et al., 2017) is an example of a joining by forming process that makes use of auxiliary joining elements whereas clinching (He, 2017) is an example of a joining by forming process that is carried out without auxiliary joining elements. Other joining by forming processes that make use of auxiliary elements and impose significant local plastic deformation in the sheets are double-sided self-pierce riveting (Kato et al., 2001), solid punch riveting (Mucha, 2013) and self-clinching fastening (Sampaio et al., 2022).

Joining by forming shares the advantage of being carried out at room temperature when compared to welding, brazing, and soldering. This allows connecting dissimilar materials and avoiding the metallurgical changes, residual stresses and distortions that inevitably result from the heat-cooling cycles.

Joining by forming also avoids the utilization of hazardous substances in both surface cleaning and bonding, but it is sensitive to formability problems that may lead to failure by cracking or instability, and may also give rise to permanent connections, to end-of-life recycling difficulties and to the necessity of using special tooling.

The fastening group includes several proven processes to fabricate lap joints and is often the preferred technology in a wide variety of applications. Bolting is the first and foremost fastening process in which standardized bolts, screws, or studs are employed to fabricate non-permanent connections between two or more overlapping sheets made from similar or dissimilar materials. Bolted lap joints are not continuous, in contrast to other types of lap joints, and are secured through direct application of non-uniform local contact pressures on the sheet surfaces through the bolts (or, screws and studs). They are easy to install and uninstall but their use is often prevented by the protrusions of the bolt's heads (and nuts) above and below the sheet surfaces and by the impact of unintentional loosening on the overall performance of the joints.

Riveting includes a set of processes in which the auxiliary elements, not the sheets, undergo extensive local plastic deformation. Riveting offers two main advantages over bolting in applications where permanent (or, semi-permanent) lap joints are admissible: (i) they do not loosen when subjected to vibration and (ii) they can secure two or more overlapping sheets with a short clamp length. Standard rivets (Fig. 2a-left) are available in a wide variety of materials and sizes and consist of a smooth cylindrical shaft with a head on one end having different possible shapes (e.g., button, universal) (Wu et al., 2021). They require holes to be drilled (or cut) in advance through the overlapping sheets so that the rivets are placed in position for subsequent compression of their headless ends (known as the 'rivet's tail'). This causes the rivet's tail to expand and create a second head that firmly holds the two sheets together.

Standard rivets are very durable, cheap, and easy to install. However, their use is often disregarded due to the low production efficiency of predrilling holes, the rivet's head protrusions located above and below the sheet surfaces, and the diminishing of locking effectiveness with the thickness of the sheets to be joined.

Blind rivets (Fig. 2a-middle) consist of two main parts: (i) a hollow sleeve with a fixed head (known as 'the rivet body') and (ii) a stem with a blind head (known as 'the rivet stem') (Wu et al., 2021). Like in conventional rivets, a hole must be predrilled through the overlapping sheets so that the blind rivet can be placed in position. Then, the rivet stem is pulled by means of a special purpose tool, causing the rivet body to be squeezed and deformed to create a mechanical interlock. The process ends when the upper part of the rivet stem breaks.

Blind rivets are mainly used in applications without access from one side (e.g., hollow, or tubular structures) but require the utilization of special tools and do not have the full strength of standard (solid) rivets.

The term 'flush rivet' is commonly used to refer to a reshaped standard rivet with a countersunk head (Wronicz et al., 2017) instead of a conventional button or universal head (Fig. 2a-right). Flush rivets are widely used in aircraft assembly due to their ability of not disturbing the aerodynamic performance of vehicles (Liu et al., 2020). Their geometry is a compromise between the tension/shear strength and the elimination of protrusions on the countersunk riveted side of the lap joints.

The typical process sequence for producing flush riveted lap joints is summarized in Fig. 2b and consists of four main stages: (i) drilling through holes in both sheets, (ii) countersinking the upper sheet with a tapered drill, (iii) inserting the flush rivet into the hole and (iv) compressing the rivet's tail to expand and create a second conventional shaped head that firmly holds the two sheets together.

Although the first and second stages can be performed automatically and even carried out in a single operation, the set-up and production run

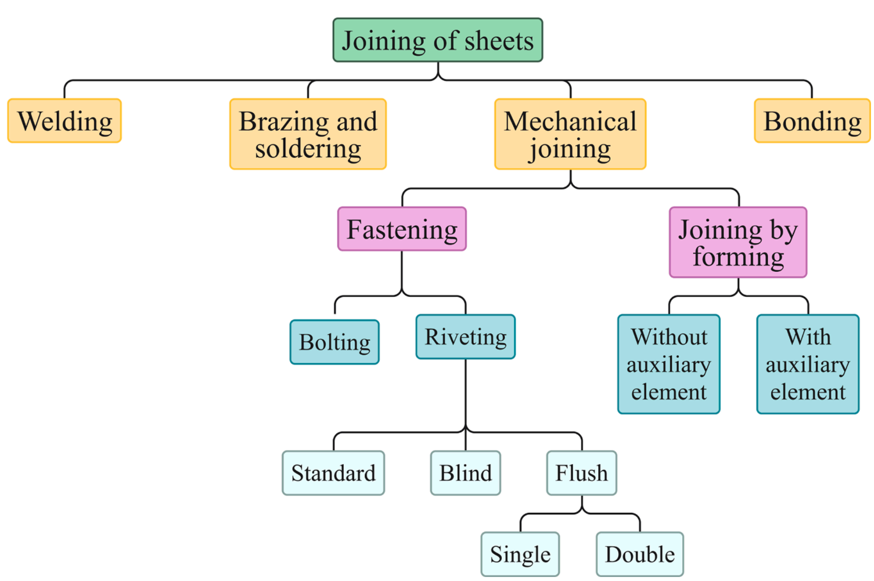

Fig. 1. Classification of the manufacturing technologies for producing lap joints in sheets.

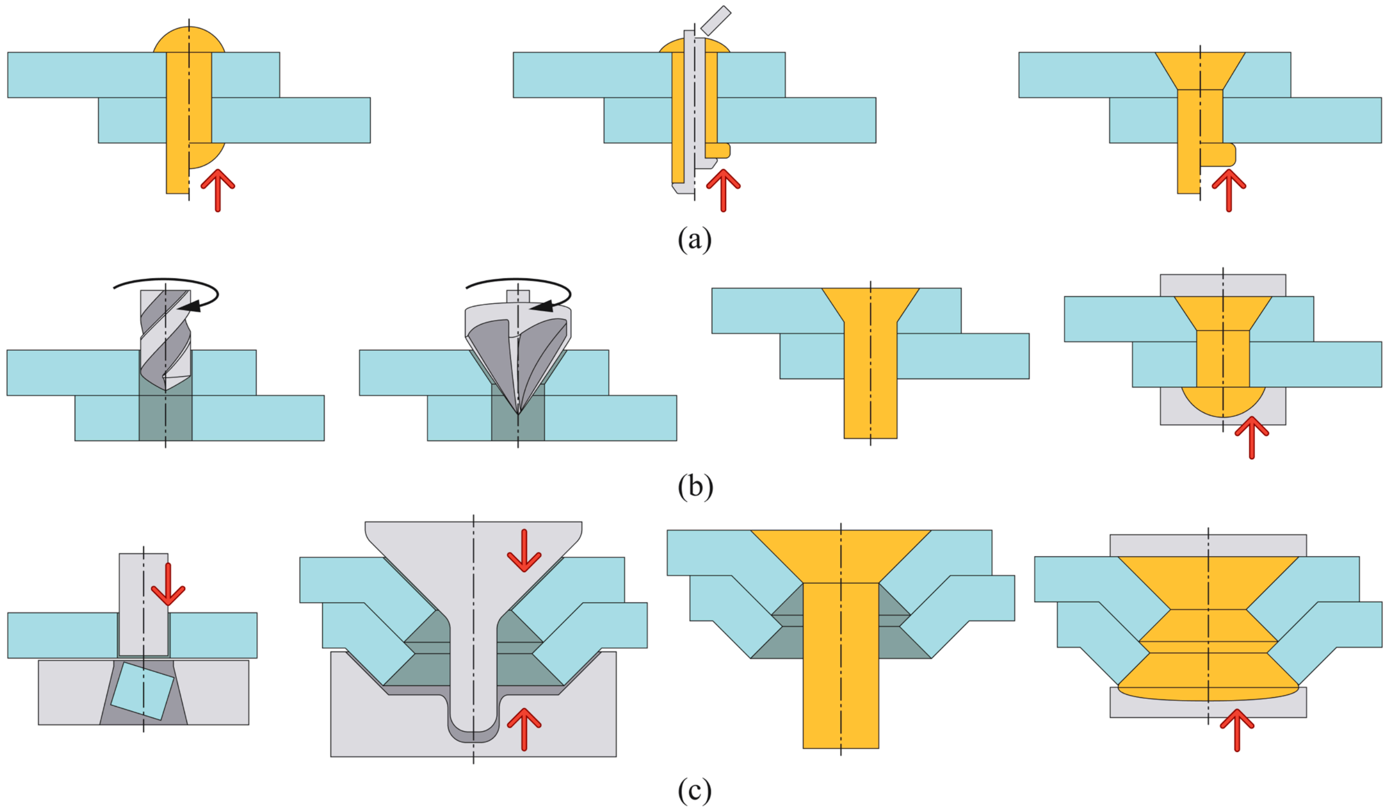

Fig. 2. (a) Different types of rivets (standard, blind and flush) and process sequence to fabricate flush-riveted lap joints by means of (b) drilling, tapered drilling, and compression and (c) punching, dimpling and compression.

time of the drilling operations have a negative impact on the productivity of the overall manufacturing route. This justifies the reason why the automotive industry has not drawn attention to riveting with flush rivets and, instead, has been widely using self-pierce riveting which can also provide a near-flat surface on one side of the lap joints.

However, even if the process sequence for producing flush riveted lap joints were modified to replace the initial drilling and tapered drilling stages by punching and countersinking with a punch and die dimpling tool (Fig. 2c) to diminish set-up and production run times, this would not allow fabricating lap joints with flat surfaces on both sides.

In fact, one of the reasons why resistance spot welding is the mainstream joining process in automotive industry (Martinsen et al., 2015) is due to its flexibility and easily automatized characteristics for creating flat, invisible lap joints (with the nugget hidden inside the sheets), despite the previous drawbacks that are inherent to the welding processes. So, the main question to be answered in this paper is about the possibility of using flush rivets to fabricate flat lap joints in the progressive or transfer multistage tools that are commonly used in the production of automotive parts?

A potential application, for example, is the connection of reinforcement elements to automotive parts fabricated by means of multiple forming operations.

This means that this paper will not focus on the extension of the process sequence of Fig. 2b to create countersunk recesses for accommodating the rivet heads in both overlapped sheets (Wenghöfer, 2011), like it is done in some electronic applications where protrusions from the object surfaces are not acceptable. Instead, it proposes a new double-flush riveting process built upon a punching-compression sequence. The process is schematically illustrated in Fig. 3 and results from looking at the morphology of the punched surfaces in a different

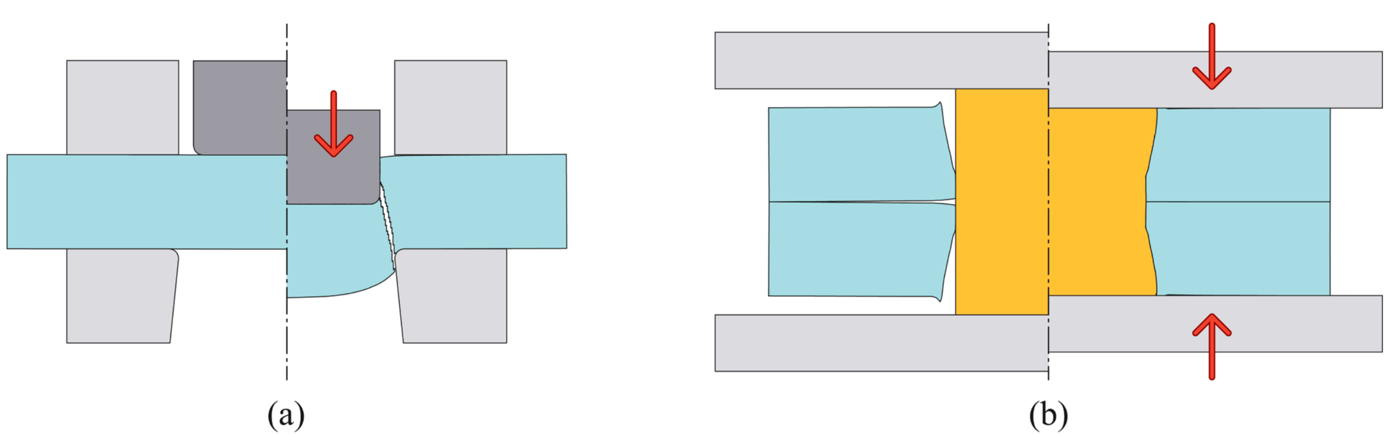

Fig. 3. The new double-flush riveting process showing the (a) punching and (b) compression operations.

perspective, in which the fracture depth and angle of the tapered cut surface are not seen as defects but as functional surfaces of countersunk holes.

For this purpose, several clearances are investigated to determine a proper angle of the tapered cut surface by simulating both the punching and compression operations that are needed to obtain a double flushed riveted joint.

Under these circumstances, this paper has a threefold objective. Firstly, to introduce a new double-flush riveting process built upon a punching-compression sequence that is suitable to fabricate flat lap joints in progressive or transfer multistage tool systems. Secondly, to present a computation procedure built upon finite element analysis of punching to select the appropriate punch-to-die clearances for subsequent compression of the solid rivets into double-flush riveted lap joints. Thirdly, to validate the new riveting process under laboratory-controlled conditions and to assess the quality of the double-flush riveted lap joints by means of destructive peel tests.

Results confirm the applicability of the new double-flush riveting process to fabricate lap joints with flat surfaces on both sides.

Methods and procedures

Mechanical and formability characterization

The lap joints were constructed from aluminum AA6082-T6 sheets with 5 mm thickness and rivets with 5 mm radius that were machined from electrolytic copper C11000 rods with 15 mm diameter. The reason for choosing copper rivets had exclusively to do with the objective of minimizing the electrical resistance of the aluminum lap joints for busbar applications. In the general case of structural applications, the choice of rivets should only be based on the principle that rivet materials must have a lower mechanical resistance than the sheet materials, so that a mechanical interlocking in the undercut area is built upon plastic deformation of the rivets instead of the sheets.

The mechanical characterization of the aluminum sheets was carried out in an Instron 4507 universal testing machine by means of tensile tests in specimens that were extracted from the sheets and tested in accordance with the ASTM standards E8/E8M (2016). Compression tests in accordance with the ASTM standards E9-89A (2000) were used to perform the mechanical characterization of the copper rods. The true stress vs. true strain curves of the sheet and rivet materials resulting from the tension and compression tests are disclosed in Fig. 4a.

The fracture forming limit curve of the aluminum AA6082-T6 was determined by the authors in a previous experimental work (Sampaio et al., 2023). The test specimens were painted with a stochastic black dot pattern covering approximately 40% of a previously painted white background so that a digital image correlation (DIC) system from Dantec Dynamics (model Q-400 3D) could be used to obtain the evolutions of the major $\varepsilon_1 = f_1(t)$ and minor $\varepsilon_2 = f_2(t)$ surface strains with time in the region of interest and to plot the corresponding strain loading paths $\varepsilon_1 = f(\varepsilon_2)$ in principal strain space . Then, by applying a methodology based on the instantaneous slopes $d\varepsilon_1/d\varepsilon_2 = \tan(\theta)$ of the strain loading paths it was possible to transform the fracture forming limit curve (i.e., the onset of failure by fracture) from principal strain space into the effective strain vs. stress triaxiality space $\bar{\varepsilon} = f(\eta)$. The methodology is described in the above-mentioned paper and the fracture forming limit curve is provided in Fig. 4b.

Both true stress vs. true strain and fracture forming limit curves will be used in the numerical modeling of double-flush riveting by punching and compression.

Experimental workplan

Validation of the new double-flush riveting process built upon a punching-compression sequence comprised two different types of experiments with unit cells that are representative of the fabrication of lap joints (Fig. 5a), at ambient temperature, under laboratory conditions. The first type of experiments involved punching with a conventional punch-die tool set (Fig. 5b), in which different clearances between the punches and dies were used to attain various morphologies of the tapered cut surfaces, namely various angles. The tool set was installed in an Instron SATEC 1200 kN hydraulic testing machine and punching was performed with a constant crosshead speed of 5 mm/min.

The second type of experiments were carried out in a punch-die tool set (Fig. 5c) in which flat compression platens plastically deformed the rivets while elastomers acted directly on the two overlapping sheets to create a double-flush mechanical interlocking in the undercut area. The use of elastomers allowed replicating the relative movements that could be alternatively obtained in double-action presses (e.g., Fig. 3b), at a lower cost. These experiments were performed in the same testing machine and used identical operating conditions to those utilized in punching.

After performing the double-flush riveting experiments, the lap joints were subjected to thermo-electrical characterization tests in accordance with the IEEE standard C37.20.2 (2015). The tests were carried out in an experimental setup that had been previously developed by authors (Pragana et al., 2023) and is schematically depicted in Fig. 5d. The setup consists of two copper block grippers to hold the lap joints along their edges and connect them to an Oficel AC transformer that supplies an electric current of 1500 A during approximately 10 min. until the temperature of the joints reaches a maximum temperature of 115 °C by Joule effect. Then, two measuring probes that are connected to a micro-ohmmeter KoCoS PROMET R600 supplying an electric current of 600 A during approximately 2 s, are used to measure the drop in

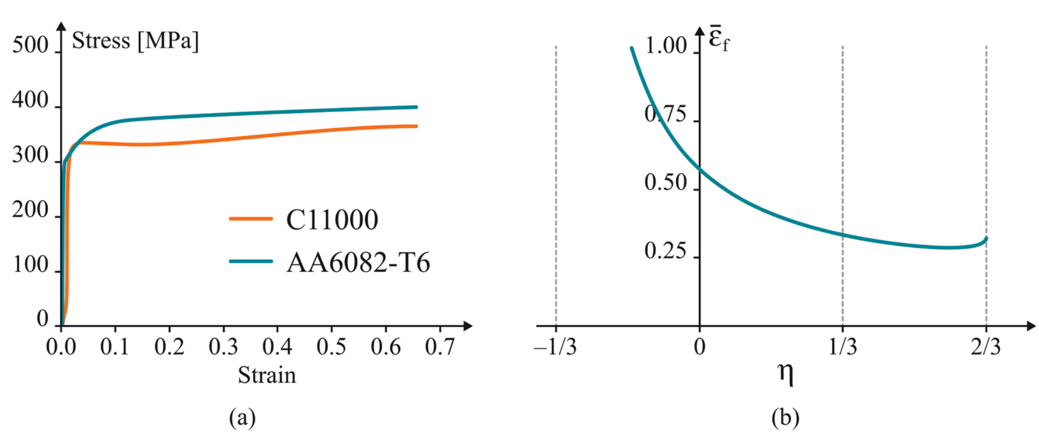

Fig. 4. (a) True stress vs. true strain curves of the aluminum AA6082-T6 and copper C11000, and (b) fracture forming limit curve of the aluminum AA6082-T6 in the effective strain vs. stress triaxiality space.

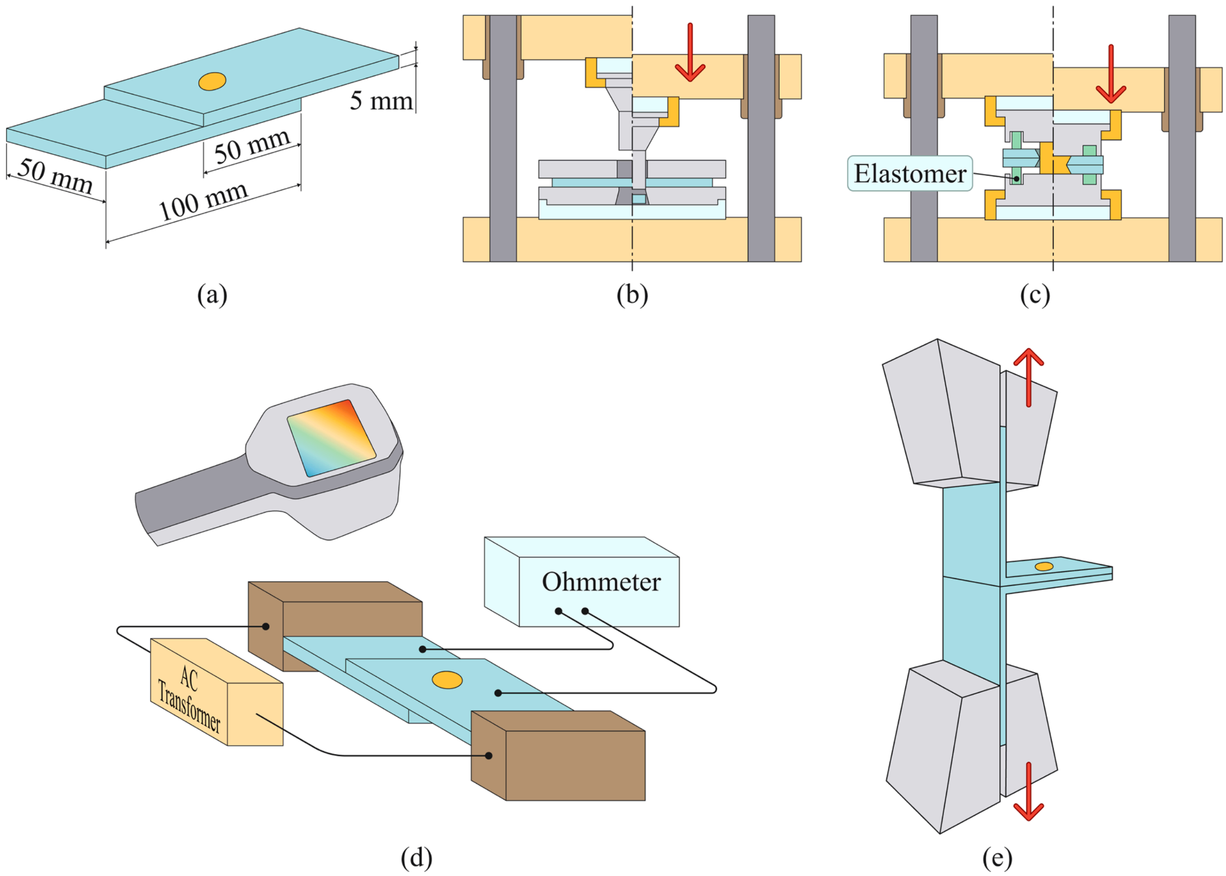

Fig. 5. Schematic representation of the experimental workplan showing (a) the unit cells, (b) the punching tool set, (c) the compression tool set, (d) the thermo-electrical measuring apparatus and (e) the setup to perform the destructive peel tests.

voltage and determine the electrical resistance of the lap joints.

After performing the thermo-electrical characterization some of the double-flush riveted lap joints were subjected to destructive peel tests (Fig. 5e) to evaluate the maximum force that the joints can safely withstand. These tests were conducted by peeling one sheet away from the other and were carried out in the Instron 4507 universal testing machine that was used in the mechanical characterization of the aluminum sheets. Due to absence of specific standards, the lap joints were prepared in accordance with the ISO Standard 14270 (2016) for resistance spot welding.

Numerical simulation

Double-flush riveting by punching and compression was numerically simulated with the in-house finite element computer program i-form (Nielsen and Martins, 2021) The program is based on the finite element flow formulation, and employs a control volume approach, with velocities u_i as the primary unknowns, of the following modified weak form of the quasi-static force equilibrium equations, which includes contact and sliding with friction between deformable and rigid objects,

$$\int_V \sigma'_{ij}\delta D_{ij}dV + \int_V \sigma_m \delta D_v dV - \int_{S_t} t_i \delta u_i dS + \int_{S_f}\left(\int_0^{|u_r|}\tau_f \delta u_r\right)dS + K_1\sum_{c=1}^{N_c} g_n^c \delta g_n^c = 0 \quad (1)$$

The first term in (1) makes use of the deviatoric Cauchy stress tensor σ'_{ij} and the rate of deformation tensor D_{ij}, whereas the second term makes use of the hydrostatic stress tensor σ_m and the volumetric rate of deformation D_v, and is numerically handled through relaxation of the incompressibility condition of the velocity field by making $\sigma_m = (K/2)D_v$, where K is a large positive number (known as the 'penalty').

The third and fourth terms in (1) correspond to the tractions t_i applied on the boundary S_t and to the frictional effects due to material sliding with a relative velocity u_r along the contact interfaces S_f. Friction is modeled by means of the law of constant friction $\tau_f = mk$, where τ_f is the friction shear stress, m is the friction factor and k is the shear flow stress.

The last term of (1) accounts for the contact between deformable objects by means of a two-pass contact search algorithm in which the N_c contact pairs are automatically extracted from the faces of the finite elements utilized in the discretization. The symbol g_n^c stands for the normal gap velocities in the contact pairs, which are penalized by a large number K_1 to avoid penetration between objects.

Further details on the implementation of the finite element flow formulation in the computer program i-form are given in Nielsen and Martins (2021).

Fig. 6 shows the typical rotational symmetric finite element models utilized in the numerical simulation of punching (Fig. 6a) and compression (Fig. 6b) at the beginning and end of each stage. The sheets and rivets were treated as deformable objects undergoing plastic deformation and their cross-sections were discretized by means of quadrilateral elements. The tools were considered as rigid objects and their contours were discretized by means of linear contact friction elements.

The initial mesh of the punching operation (Fig. 6a) made use of localized refinement to correctly capture damage localization at the beginning of the process. Localized refinement was replaced with a global finer mesh after the first remeshing operation aimed at eliminating excessive distortion of elements with all the history-dependent

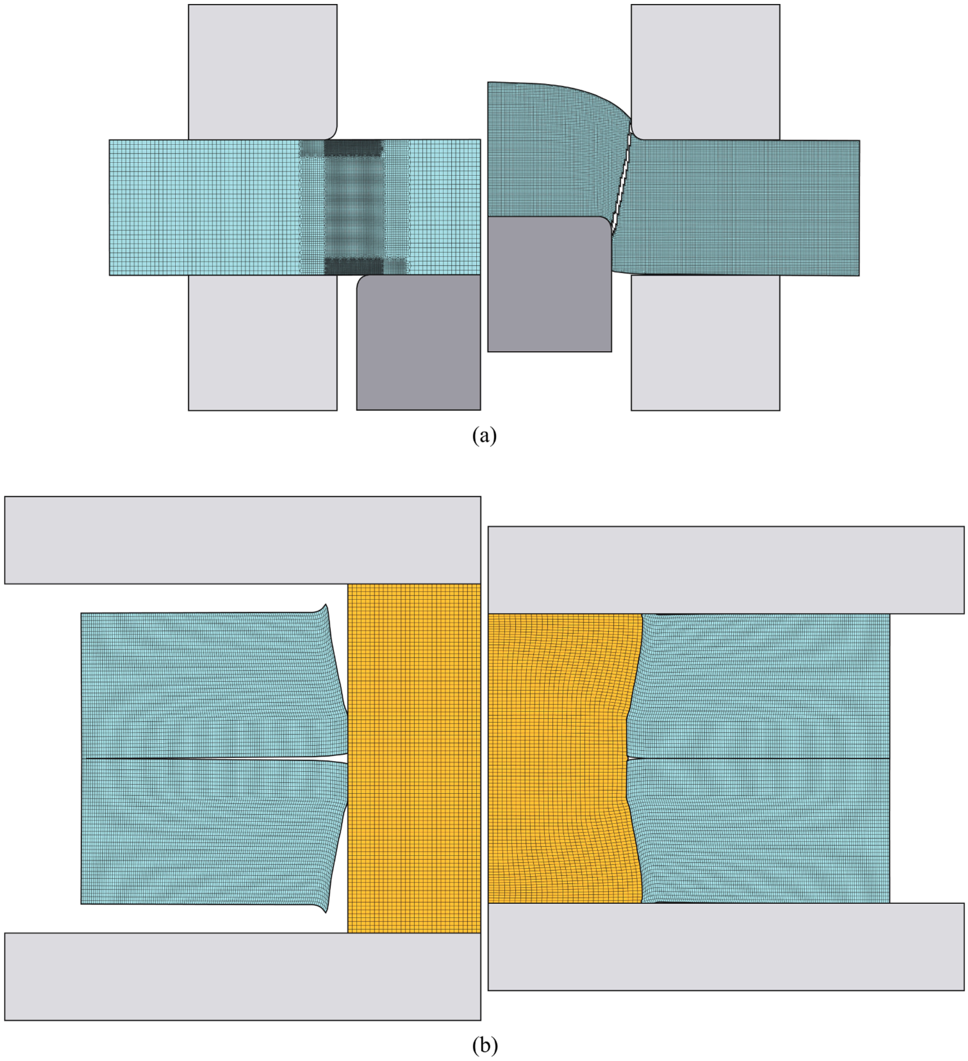

Fig. 6. Initial and final computed meshes of double-flush riveting for the (a) punching stage with a punch-to-die clearance of 0.8 mm and for the subsequent (b) compression stage at the beginning (left) and end (right).

variables transferred from the initial to the new mesh. Several remeshings were carried out before and after crack triggering and propagation. The latter was numerically handled by means of an element deletion technique built upon the normalized Cockcroft-Latham (1968) ductile fracture criterion,

$$D_{crit} = \int_0^{\overline{\varepsilon}_f} \frac{\sigma_1}{\overline{\sigma}} d\overline{\varepsilon} \tag{2}$$

where σ_1 is the major principal stress and $\overline{\sigma}$ is the effective stress. $D_{crit} = 0.675$ is the critical value of the ductile fracture criterion (2) at the onset of cracking that replicates the experimental fracture forming limit curve plotted in Fig. 4b.

The 'staircase contour' of the tapered cut surface resulting from the element deletion technique was smoothed by means of a spline fitting before starting the compression stage (Fig. 6b). A remeshing was additionally performed to create a new mesh without excessive distorted elements. No further remeshings were necessary until the end of the compression stage.

Results and discussion

Preliminary modeling

The success of double-flush riveting by punching and compression is very much dependent on the morphology of the punched surfaces, namely on the tapered cut surface (also known as the 'breakout angle'). In fact, while in some punching applications the breakout angle is unacceptable and requires removal by subsequent shaving, in double-flush riveting the whole idea is built upon the breakout angle due to its resemblance with a countersunk hole opened with a tapered drill.

Fig. 7 shows the finite element predicted surfaces after punching the aluminum AA6082-T6 sheets with different punch-to-die clearances. The cracks were triggered for different punch strokes at the regions where the accumulated damage D associated with the normalized Cockcroft-Latham (1968) ductile fracture criterion reaches the critical value $D_{crit} = 0.675$ (refer to 'Mechanical and formability characterization' and to 'Numerical simulation').

The breakout angles were created by crack propagation and are directly dependent on the punch-to-die clearances. As seen, while a clearance of 0.5 mm (corresponding to 10% of the sheet thickness), is suitable for conventional punching because it gives rise to a breakout angle of approximately 7° (Fig. 7a), a larger clearance value of 0.8 mm (corresponding to 16% of the sheet thickness) is considered unsuitable

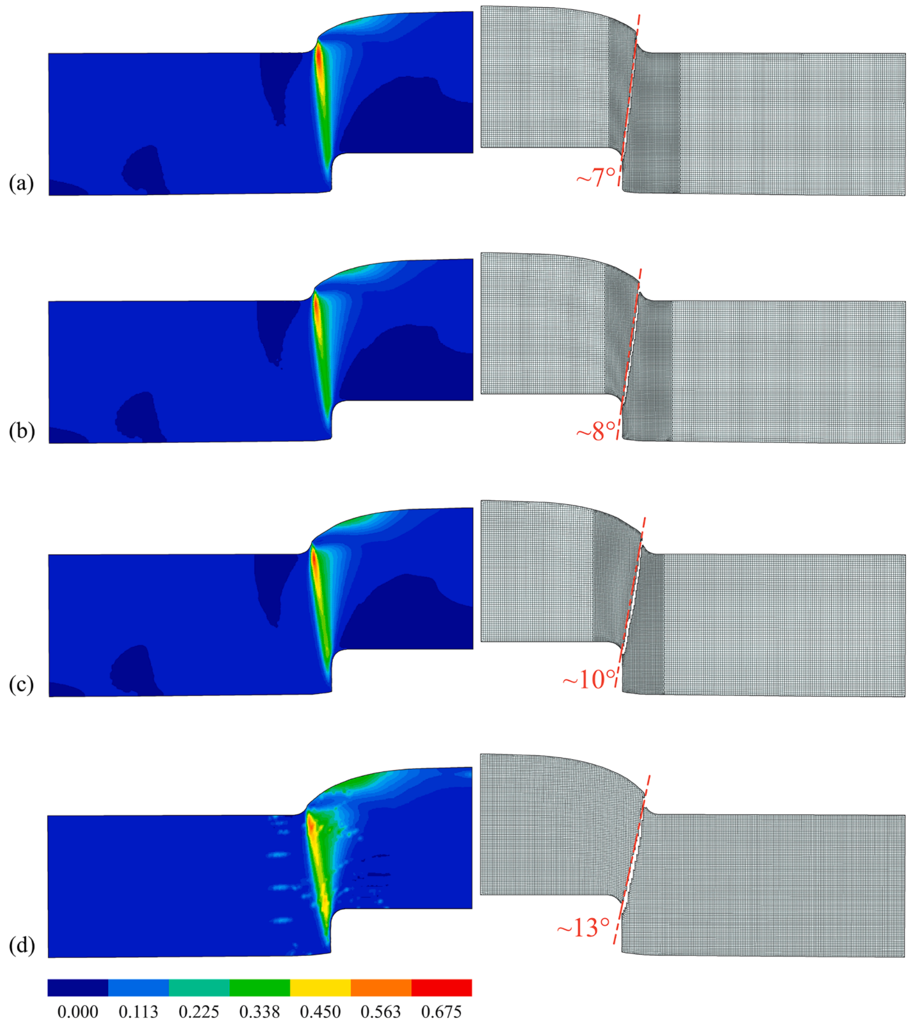

Fig. 7. Finite element predicted cross section of the punched surfaces with (left) the distribution of accumulated ductile damage according to the normalized Cockcroft-Latham ductile fracture criterion at the onset of cracking and (right) the values of the breakout angles for punch-to-die clearances of (a) 0.5 mm, (b) 0.6 mm, (c) 0.7 mm and (d) 0.8 mm.

for punching applications because it creates a breakout angle of 13° (Fig. 7d).

However, the increase of the breakout angle with the punch-to-die-clearance that is shown in the finite element computed cross sections of Fig. 7a to d, gives rise to punch surfaces closer to countersinking and, therefore, appropriate for double-flush riveting.

The left-side images in Fig. 8 show the finite element predicted cross sections of the double-flush riveted lap joints after unloading (i.e., after removing the compression tools). As seen, punching with larger clearances allows bigger undercuts to be obtained during the compression stage, in which the rivet heads are fully accommodated below the sheet surfaces. The undercuts give rise to form-closed joining by mechanical interlocking.

The right-side images in Fig. 8 show the corresponding distribution of (residual) radial stress after unloading. As seen, the compressive normal stresses (pressures) along the contact interface between the rivet and sheets increase with the initial punching clearance and give rise to an additional force-close joining mechanism that adds to the previously mentioned form-closed.

Experimental validation

Experimental validation of double-flush riveting involved fabrication of lap joints in laboratory conditions using the new proposed punching-compression sequence. Fig. 9 shows the experimental and finite element predicted cross sections of an aluminum AA6082-T6 sheet with 5 mm thickness that was punched with a punch-to-die clearance of 0.8 mm. The experimental values included in the figure are mean values resulting from five different samples and measured at different locations of the hole perimeter. The agreement is excellent with almost identical values of the experimental and numerically predicted breakout angles.

The detail on the right side of Fig. 9 shows the 'staircase' profile resulting from the element deletion technique that was utilized in the numerical modeling of crack propagation.

Fig. 10 shows the actual and finite element predicted cross sections of a lap joint made from two aluminum AA6082-T6 overlapping sheets that were punched with a punch-to-die clearance of 0.8 mm and subsequently connected with a cylindrical rivet with 5 mm radius made from copper C11000. The detail on the left side shows the numerically predicted contact interface between the rivet and the cut surfaces of the overlapped sheets. The overall agreement is good and proves the applicability of the new riveting process to fabricate lap joints with flat surfaces on both sides.

The force vs. displacement evolutions during the punching and compression stages are shown in Fig. 11. The agreement is good in both stages with major differences found in punching, namely in the peak force and initial force growth rate whose experimental values are slightly smaller than the numerically predicted ones. These differences

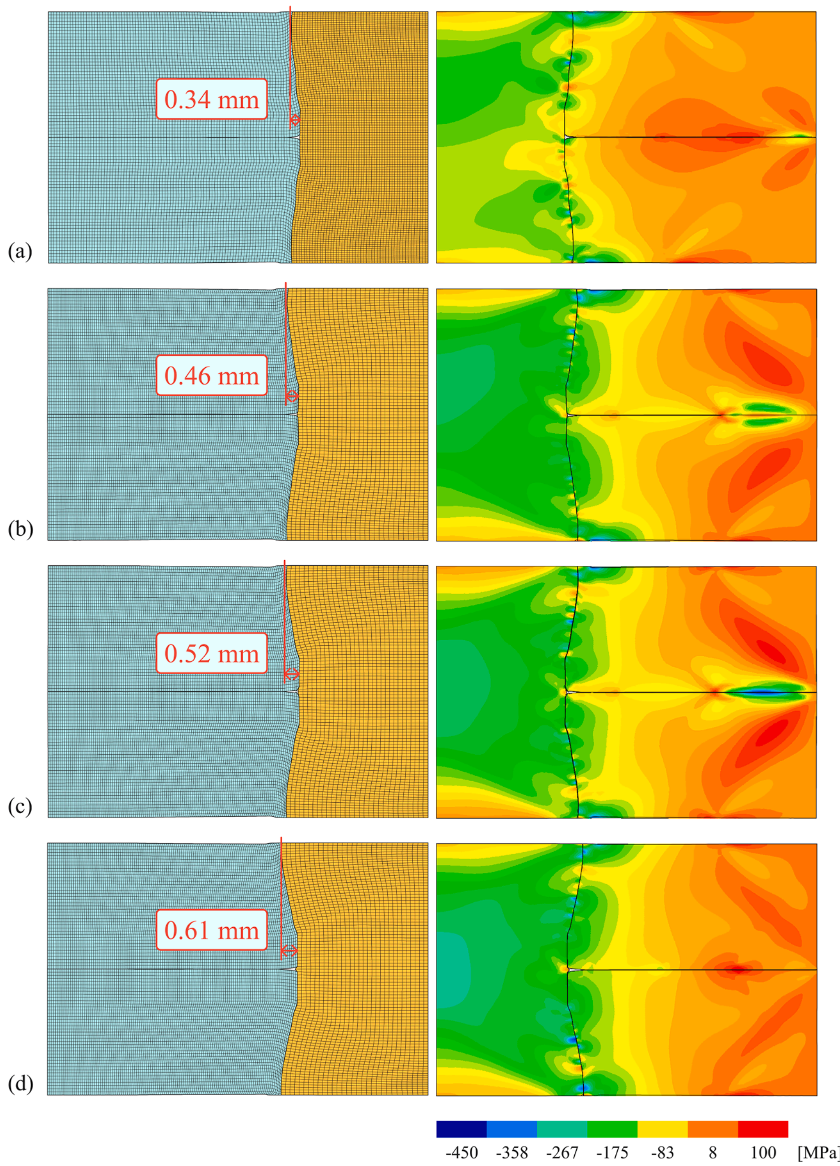

Fig. 8. Finite element predicted cross section of the double-flush riveted lap joints after unloading showing (left) the undercuts and (right) the distribution of radial stress (MPa) for punch-to-die clearance values of (a) 0.5 mm, (b) 0.6 mm, (c) 0.7 mm and (d) 0.8 mm.

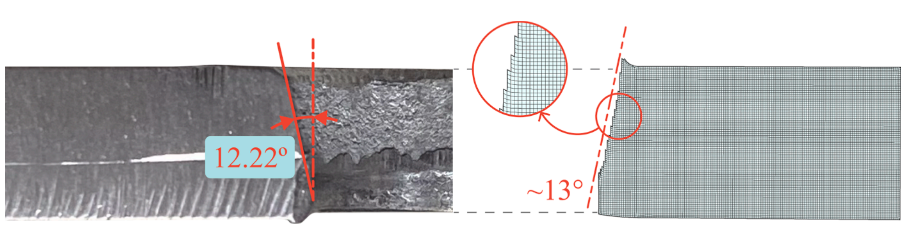

Fig. 9. Experimental and finite element predicted cross sections of an aluminum AA6082-T6 sheet that was punched with a punch-to-die clearance of 0.8 mm. Values refer to the breakout angle.

are attributed to minor punch-to-die variations within the tolerance range of the solid rivet diameters.

In what concerns the compression stage, the force vs. displacement evolution presents some resemblance with that commonly found in closed die forging processes, in which the force grows, slowly at first, in an almost proportional way, and steeply at the end of the punch stroke. The first part is related to the compression of the rivet ends, which expand freely along the circumferential direction, while the last part is caused by the contact of the rivet with the cut surfaces of the overlapped sheets. A maximum force of approximately 200 kN was obtained for the test case shown in Fig. 11.

Post-fabrication tests

The experimental workplan included two post-fabrication tests. One of these tests had specifically to do with the utilization of double-flush

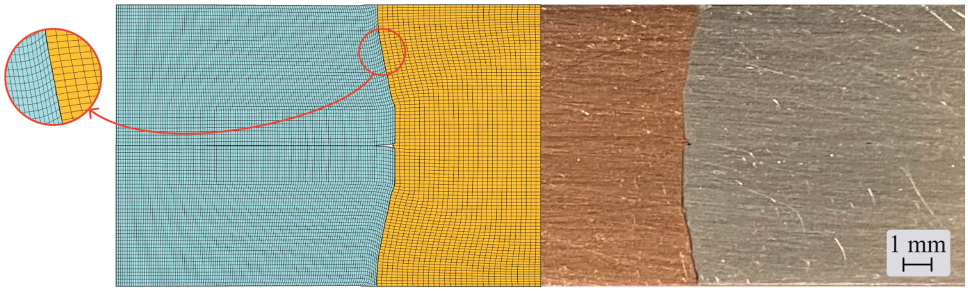

Fig. 10. Finite element predicted geometry and photograph of the cross section of a double-flush riveted lap joint made from two aluminum AA6082-T6 sheets and a C11000 copper rivet. The sheets were punched with a punch-to-die clearance of 0.8 mm.

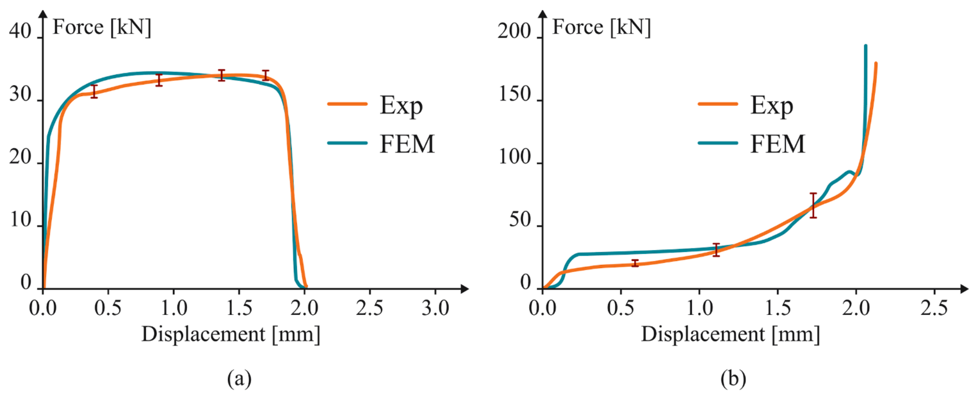

Fig. 11. Experimental and finite element predicted evolution of the force with displacement for the (a) punching and (b) compressions stages of the double-flush riveted lap joint of Fig. 10.

riveted lap joints in busbars for energy distribution systems and consisted of performing the thermo-electrical characterization of the lap joints according with the methods and procedures that were previously described in 'Experimental workplan' (refer to Fig. 5d). The result is given in Fig. 12 and allows the conclusion that the electrical resistance of the joints increases linearly with temperature like the electric resistivity of aluminum and copper.

Results also show that the electrical resistance of double-flush riveted lap joints is 24% to 30% higher than that of ideal lap joints, in which the aluminum sheets are in perfect contact along their overlapped surfaces, without contaminants, oxide films or auxiliary joining elements. This result is very good when compared to that of conventional fastened joints, which are also included in Fig. 12.

The electrical resistance of the fastened and ideal lap joints was obtained by experimentation and finite element analysis, respectively, and were retrieved from a previous work of the authors (Pragana et al., 2023).

The other post-fabrication test is the destructive peel test to determine the maximum peel strength that double-flush riveted lap joints can safely withstand (refer to Fig. 5e). Fig. 13 shows the experimental evolution of the force with displacement during the peel test and a photograph containing a detail of the observed failure mode. As seen, the first irreversible movement of the lap joint occurs at approximately 2 kN and is followed by a substantial amount of deformation up to the peak value

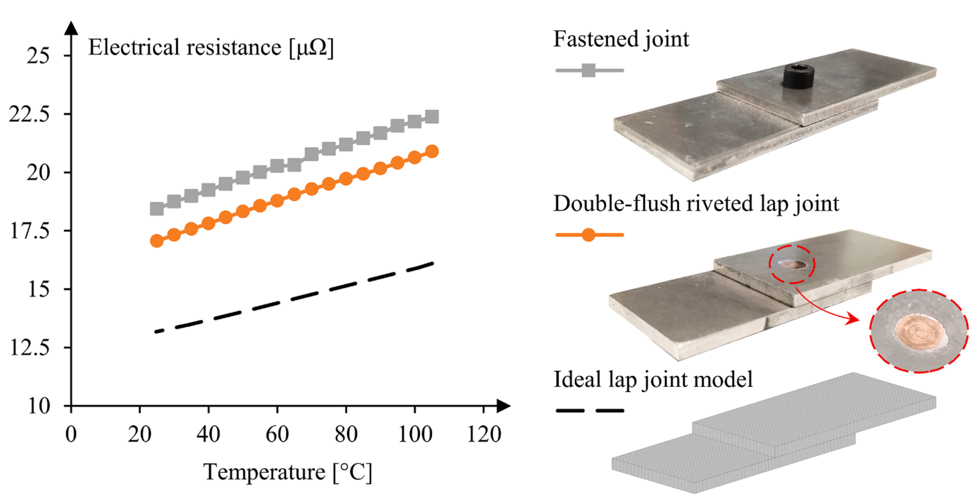

Fig. 12. Experimental evolution of the electrical resistance with temperature for double-flush riveted, fastened, and ideal lap joints. Photographs show the corresponding unit cells and the ideal lap joint model utilized in finite element modeling.

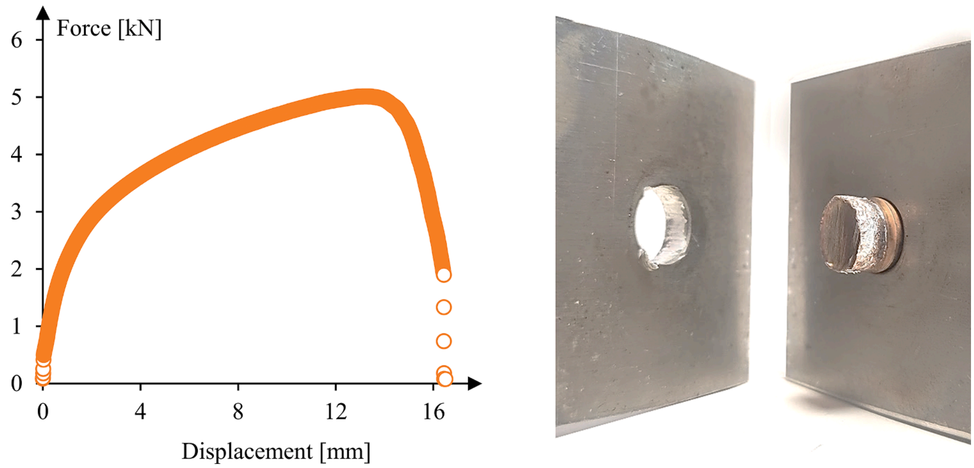

Fig. 13. Experimental evolution of the force vs. displacement for the destructive peeling tests of the double-flush riveted lap joints made from two overlapping aluminum AA6082-T6 sheets connected with a copper C11000 rivet. The photograph shows a detail of the unit cell after testing.

of 5 kN, due to bending of the sheets when they are progressively peeled away from each other.

The sudden drop of the force is caused by a pullout failure mechanism (refer to the photograph) that is caused by the force being heavily concentrated on one side of the rivet.

Conclusions

Double-flush riveting by punching and compression can be successfully used to fabricate flat lap joints in which the rivet heads are fully accommodated below the sheet surfaces. The process can be easily integrated in progressive or transfer multistage tool systems and special emphasis must be put on the selection of the sheet and rivet materials and on the choice of the punch-to-die clearance for the punching operation.

In the case of material selection, the main rule is to choose rivets with a lower mechanical resistance than the sheets, so that mechanical interlocking in the undercut area is built upon plastic deformation of the rivets instead of the sheets.

In the case of punch-to-die clearance, results show that large values with some loss of surface evenness, which are generally inappropriate for conventional blanking operations, are preferred because they allow obtaining good mechanical interlocking in the undercut area during the compression (riveting) operation. A punch-to-die clearance corresponding to 16% of sheet thickness proved appropriate to join aluminum AA6082-T6 sheets of 5 mm thickness with copper C11000 rivets of 5 mm radius. The required force during the riveting process was below 200 kN and its evolution trend with a steep increase at the end, when the rivet surface gets into contact with the cut surfaces of the overlapping sheets, can be easily used to the control the process.

Destructive peel tests showed that double-flush riveted joints fail by pullout after reaching a peak force of 5 kN. The thermo-electrical characterization of the joints allowed concluding that the electrical resistance increases with temperature and that their values are 24% to 30% higher than those obtained for an ideal lap joint but smaller than those obtained for a fastened joint made from the same sheet materials.

Declaration of Competing Interest

The authors declare that they have no known competing financial interests or personal relationships that could have appeared to influence the work reported in this paper.

Data availability

Data will be made available on request.

Acknowledgments

The authors would like to acknowledge the support provided by Fundação para a Ciência e a Tecnologia of Portugal and IDMEC under LAETA- UIDB/50022/2020 and PTDC/EME-EME/0949/2020. Rui Sampaio would also like to acknowledge the support under the PhD Studentship 2022.12351.BD.

References

ASTM E8/E8 M, 2016. Standard Test Methods for Tension Testing of Metallic Materials. ASTM International, West Conshohocken, USA.
ASTM E9-89A, 2000. Standard Test Methods of Compression Testing of Metallic Materials at Room Temperature. ASTM International, West Conshohocken, USA.
Brandon, D., Kaplan, W.D., 1997. Joining Processes: an Introduction. John Wiley & Sons, Chichester, UK.
Cockroft, M.G., Latham, D.J., 1968. Ductility and the workability of metals. J. Inst. Met. 96, 33–39.
He, X., 2017. Clinching for sheet materials. Sci. Technol. Adv. Mater. 18, 381–405.
IEEE Std C37.20.2, 2015. IEEE Standard for Metal-Clad Switchgear. IEEE Power and Energy Society, New York, USA.
ISO Std 14270, 2016. Resistance Welding - Destructive Testing of Welds - Specimen dimensions and Procedure for Mechanized Peel Testing Resistance Spot, Seam and Embossed Projection Welds. ISO - International Organization for Standardization, Geneva, Switzerland.
Kato, K., Okamoto, M., Yasuhara, T., 2001. Method of joining sheets by using new type of rivets. J. Mater. Process. Technol. 111, 198–203.
Li, D., Chrysanthou, A., Patel, I., Williams, G., 2017. Self-piercing riveting - a review. Int. J. Adv. Manuf. Technol. 92, 1777–1824.
Liu, J., Zhao, A., Liu, Y., Dong, H., Bi, Y., 2020. Numerical and experimental investigation on the rivet head flushness in automatic countersunk riveting. Int. J. Adv. Manuf. Technol. 110, 395–411.
Martinsen, K., Hu, S.J., Carlson, B.E., 2015. Joining of dissimilar materials. CIRP Ann. Manuf. Technol. 64, 679–699.
Meschut, G., Merklein, M., Brosius, A., Drummer, D., Fratini, L., Füssel, U., Gude, M., Homberg, W., Martins, P.A.F., Bobbert, M., Lechner, M., Kupferf, R., Groger, B., Han, D., Kalich, J., Kappe, F., Kleffel, T., Kohler, D., Kuball, C.M., Popp, J., Romisch, D., Troschitz, J., Wischer, C., Wituschek, S., Wolf, M., 2022. Review on mechanical joining by plastic deformation. J. Adv. Join. Process. 5, 100113.
Mucha, J., 2013. The effect of material properties and joining process parameters on behavior of self-pierce riveting joints made with the solid rivet. Mater. Des. 52, 932–946.
Nielsen, C.V., Martins, P.A.F., 2021. Finite Element Flow Formulation in Metal Forming: Formability, Simulation and Tool Design. Academic Press, London, UK, pp. 181–249.
Pragana, J.P.M., Sampaio, R.F.V., Chantreuil, J., Bragança, I.M.F., Silva, C.M.A., Martins, P.A.F., 2023. Double-sided injection lap riveting. Int. J. Adv. Manuf. Technol. 125, 3241–3253.
Sampaio, R.F.V., Pragana, J.P.M., Bragança, I.M.F., Silva, C.M.A., Martins, P.A.F., 2022. A self-clinching fastener for hidden lap joints. CIRP J. Manuf. Sci. Technol. 37, 434–442.

Sampaio, R.F.V., Pragana, J.P.M., Bragança, I.M.F., Silva, C.M.A., Nielsen, C.V., Martins, P.A.F., 2023. Characterization of the fracture forming limits by radial extrusion. J. Manuf. Mater. Process. 7, 107.

Wenghöfer, F., 2011. Methodische Anleitung für den Lehrenden Nieten. Institut für berufliche Entwicklung, Berlin.

Wronicz, W., Kaniowski, J., Malicki, M., Kucio, P., Klewicki, R., 2017. Experimental and numerical study of NACA and conventional riveting procedure. Fatigue Aircr. Struct. 3917, 157–170.

Wu, J., Chen, C., Ouyang, Y., Qin, D., Li, H., 2021. Recent development of the novel riveting processes. Int. J. Adv. Manuf. Technol. 117, 19–47.